

Short Communication

Rate Performance Enhancement of Anode for Lithium-Ion Battery via Composition of Hard Carbon And Silicon-Carbon Nanofiber

Tae-Hwan Park¹, Jae-Seong Yeo¹, Yuzo Ohata¹, Min-Hyun Seo², Jin Miyawaki², Isao Mochida³, Seong-Ho Yoon^{1,2,*}

¹ Interdisciplinary Graduate School of Engineering Sciences, Kyushu University, Kasuga 6-1, Fukuoka, 816-8580, Japan

² Institute for Materials Chemistry and Engineering, Kyushu University, Kasuga 6-1, Fukuoka, 816-8580, Japan

³ Research and Education Center of Carbon Resources, Kyushu University, Kasuga 6-1, Fukuoka, 816-8580, Japan

*E-mail: yoons@cm.kyushu-u.ac.jp

Received: 22 October 2012 / Accepted: 22 November 2012 / Published: 1 January 2013

The internal-pore introduced hybridized materials with hard carbon and specially prepared silicon-carbon nanofiber composite have been prepared from mechanical mixing and continuous carbonization processes. The effective additions of 10–30 wt% of silicon-carbon nanofiber composites into hard carbon matrix improved the rate performance as well as discharge capacity very much. The prepared hybridized materials through the 10 and 30 wt% addition of the silicon-carbon nanofiber composites into hard carbons showed the discharge capacity retention rates of over 87.8% and 89.4% even at 3,000 mA g⁻¹ (over 6C) and high discharge capacities of 337 and 441 mAh g⁻¹, respectively. The artificial introduction of the appropriate amounts internal pores into hard carbon matrix with silicon-carbon nanofiber composite can effectively enhance the high rate performance as well as the discharge capacity without compromising the 1st cycle coulombic efficiency.

Keywords: Hard carbon, Rate performance, Si-Carbon nanofiber composite, Internal pores, Li-ion battery

1. INTRODUCTION

Recently, Li-ion batteries (LIB) for the application of electric vehicle and hybrid electric vehicles get a public interest. Present LIBs use graphite as anodic materials, which have many advantages including stable cycle performance and low cost. However, graphite is not satisfied as an

anode to use for high power density application due to their insufficient rate performance [1]. Therefore, hard carbon materials have been investigated due to their relative higher rate performance compared to graphite [2, 3]. However, hard carbon materials suffer from large irreversible capacities due to the formation of solid electrolyte interface (SEI) on the surface of hard carbons [4] and also unsatisfied with their insufficient discharge capacity to meet with recent severe requirements of electric vehicle and digital devices. Studies on hard carbon materials indicate that the existence of internal pores shows significant effect on the electrochemical performance, such as improved rate performance because they are considered to have the reasonable pore structure as much shorter ion transfer pathways [5-11].

In this study, we propose a significant role of internal pores which are artificially introduced in the hard carbon matrix with very specially designed silicon-carbon nanofiber (Si/CNF) through the mechanical mixing and continuous carbonization processes. The prepared Si/CNF contained hard carbon hybridized materials carry adequate internal pores and exhibit excellent cyclability, discharge capacity and rate performance as anode for Li-ion battery with maintaining high 1st cycle coulombic efficiency due to their low surface area.

2. EXPERIMENTAL PART

2.1. Chemicals and material

Nano-sized silicon particles with average diameter of 50 nm (Nanostructured & Amorphous Materials Inc., Houston, TX) and ethylene bottom oil (EO, SK Co. Ltd., Seoul, Korea)-derived pitch were used as starting materials in this study. High-purity helium (He, 99.95 %), methane (CH₄, 99.999 %), carbon monoxide (CO, 99.95 %), and hydrogen (H₂ 99.99999 %) (Asahi Sanso Co. Ltd., Japan) were applied for the pyrolytic carbon (PyC) and CNF growths. The PyC coating on the Si particles was carried out in a horizontal furnace using a quartz boat at atmospheric pressure as follows. To begin with, the Si particles were heated at heating rate of 10°C min⁻¹ under a He gas flow. When temperature reached to 900°C, the gas flow was changed to mixed gases of CH₄ and H₂ (4:1, vol/vol), and maintained for 1 h to well-coat the surface of the Si particles by PyC. The reactor was cooled down to room temperature in a He gas flow. The amount of the coated PyC on the 50 nm Si particles was carefully controlled to 20 wt% on the PyC-coated 50 nm Si (SP) weight base (amount of PyC (%) = Increased weight after PyC coating / Input Si particles weight). Reagent grade iron nitrate enneahydrate [Fe(NO₃)₃·9H₂O] (Wako chemical Co. Ltd., Japan) was used as a precursor of the CNF growth catalyst. The Si particles were dispersed into Fe(NO₃)₃·9H₂O/ethanol solution, and then the slurry was stirred for 3 h at room temperature. The amount of the catalyst was carefully controlled to support 2 wt% Fe. After evaporating ethanol at 60°C, these mixtures were dried at 105°C for 6 h in vacuum. The SP with Fe (2 wt%) was placed in the center of a horizontal tube furnace and heated to 600°C at the heating rate of 10°C min⁻¹ in a He gas flow at atmospheric pressure. Then, the mixed gases of CO and H₂ were introduced, and kept flowing for 30 min. The reactor was cooled down to room temperature in a He gas flow after the CNF synthesis. The amount of CNF growth was

controlled to 22 wt% on the SP weight basis (amount of CNF (%) = Increased weight after CNF growth / Input SP particles weight). The composite of 50 nm Si/PyC/CNF (SPC) and hard carbon was prepared as follows; SPC and EO-derived pitch were mixed in tetrahydrofuran (THF) and dried at 80°C for 12 h in a vacuum oven. The EO-derived pitch and the mixtures were then heated at 800°C for 1 h followed by heat treatment (carbonization) up to 1000°C at 10°C min⁻¹ of heating rate under vacuum condition of 20 Pa. Thus prepared specimen was designated as HC from the EO-derived pitch and SPC/HCX from the mixtures, where X indicates mixing ratio of HC on a weight basis. Figure 1 shows a schematic model of Si/PyC/CNF particles, and the hybridized material of Si/PyC/CNF with hard carbon.

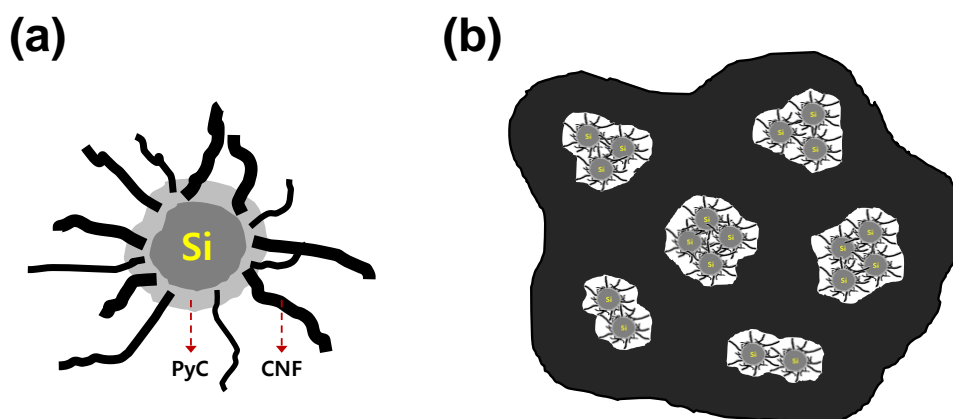


Figure 1. A schematic model of (a) Si/PyC/CNF particles, and (b) the hybridized material of Si/PyC/CNF with hard carbon.

2.2. Analysis and electrochemical measurement

Surface area analysis was carried out using the Brunauer-Emmett-Teller (BET) nitrogen adsorption method (4200e, Nova, Japan). The surface morphology was observed using a scanning electron microscope (SEM, JSM-6700F, JEOL, Japan). Crystallographic properties were measured by an X-ray powder diffractometer (CuK α , Ultima-III, Rigaku, Japan). The apparent density was estimated by the n-butanol displacement method. The galvanostatic charging and discharging were carried out using coin-type cells of CR2032 with two electrodes, where Li metal foil was used as a counter electrode, styrene-butadiene rubber (SBR, trade name BM-400B, ZEON, Japan) as a binder, and carboxy methyl cellulose (CMC) as a thickening agent system (anode material:SBR:CMC = 90:7:3, wt%). To form the anode electrode, the mixed slurry was coated on a copper foil (18 μ m thick), dried at 120°C under vacuum for 12 h, pressed using a roll-type mill under 100 MPa of pressure, cut into discs (12 mm in diameter and about 40 μ m in thickness), and then, weighed by using an ultra-fine balance to adjust the amount of active material. Coin-type cells were assembled in an Ar-filled glove box using a polyethylene film (16 μ m thick) as a separator and 1M LiPF₆ in ethylene carbonate (EC)/diethyl carbonate (DEC) (1:1 vol%, Ube Kosan, Japan) as an electrolyte. The electrochemical

measurements were performed through charging and discharging at constant current (CC) with the current density of 30 or 100 mA g⁻¹ in the potential range of 0-1.5 V versus Li/Li⁺ (Toscat-3100, Toyo-system, Japan) at room temperature.

3. RESULTS AND DISCUSSION

3.1. Analytical results

Figure 2 (a) – (d) shows the SEM images of HC and SPC/HC composites. HC, SPC/HC90 and SPC/HC70 showed very smooth surfaces in figure 2 (a) – (c), but SPC/HC50 did relatively rough surface with large pores in figure 2 (d).

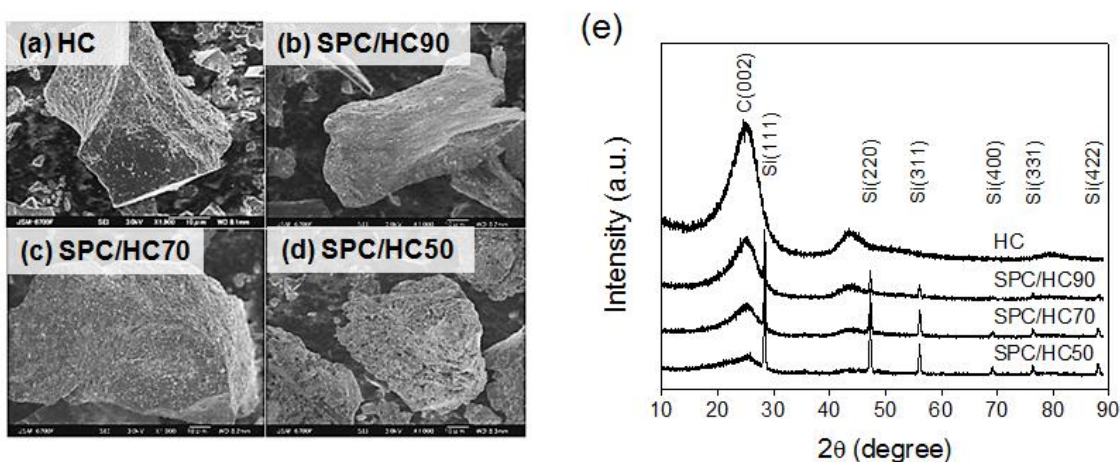


Figure 2. (a) – (d) SEM images and (e) XRD profiles of HC and SPC/HC composites.

The XRD profiles of HC and SPC/HC composites are shown in figure 2 (e). The peak near 25°, which is attributed to the (002) layer of the carbon, is broad regardless of the mixing ratio of HC, revealing that the hard carbon matrix was not well-graphitized [12]. This peak became predominant with increasing HC ratio in the SPC/HC composites. Silicon also exhibits clear peaks at about 28.5°, 47.4°, 56.2°, 69.2°, 76.5°, 88.0°, which are indicated to (111), (220), (311), (400), (331) and (422) planes of crystalline silicon, respectively [13, 14].

The surface area of the HC and SPC/HC composites are shown in table 1. BET surface areas decrease as increasing HC ratio in the HC and SPC/HC composites. X-ray density [15] of carbon components of the specimens and particle density are evaluated from XRD and n-butanol displacement measurement as shown in table 1. As the increment of the SPC content, d_{002} values increase from 3.641 Å to 3.573 Å and therefore the X-ray density calculated from d_{002} data increases from 2.043 g cm⁻³ to 2.081 g cm⁻³. On the other hand, the particle density estimated from n-butanol displacement method decreases as increasing the SPC addition amount from 1.723 g cm⁻³ to 1.354 g cm⁻³. And the particle density except silicon could be calculated by removing the portion of silicon density in the

PC/HC composites. From these two density data, the internal pore volume is calculated by equation: $E = 1/D - 1/A$. The internal pore volumes of the HC and SPC/HC composites increased with a decrement of the SPC addition amount from $0.091 \text{ cm}^3 \text{ g}^{-1}$ and $0.400 \text{ cm}^3 \text{ g}^{-1}$. The increased internal pore volume is also estimated from the difference of internal pore volume between the HC and SPC/HC composites. The increased internal pore volumes of SPC/HC composites also increase as decreasing of the SPC addition amount from $0.064 \text{ cm}^3 \text{ g}^{-1}$ (70%) and $0.354 \text{ cm}^3 \text{ g}^{-1}$ (385%) as the comparison of the HC matrix.

Table 1. Compositions, surface areas, d_{002} data, X-ray density, particle density and internal pore volume of the HC and SPC/HC composites.

Sample	Composition (wt %)		Surface area (m^2/g , N ₂ -BET)	d_{002} (Å)	X-ray density (g/cm^3 , A)	Particle density (g/cm^3 , B)	Silicon ratio ^a (C)	Particle density except silicon ^b (g/cm^3 , D)	Internal pore volume ^c (cm^3/g , E)	Increased internal pore volume ^d (cm^3/g , F)
	SPC	HC								
HC	0	100	6	3.641	2.043	1.723	-	1.723	0.091	-
SPC/HC90	10	90	7	3.593	2.070	1.627	0.062	1.588	0.146	0.064 (70 %)
SPC/HC70	30	70	20	3.584	2.075	1.488	0.186	1.376	0.244	0.180 (196 %)
SPC/HC50	50	50	27	3.574	2.081	1.354	0.310	1.135	0.400	0.354 (385 %)

^a Density of silicon: 2.33 g cm^{-3} ^b $D = (B - B \times C) / (1 - (B - B \times (1 - C))) / 2.33$

^c $E = 1/D - 1/A$ ^d $F = E(\text{SPC/HC}) - E(\text{HC}) \times \text{Composition}(\text{of HC in SPC/HC}) / 100$

3.2. Electrochemical properties

The cyclability and rate performance of the HC and SPC/HC composites are shown in figure 3. In figure 3 (a), the cyclability of the SPC/HC composites is improved with an increment of the HC amount. And the discharge capacity of the SPC/HC composites is increased as increasing the SPC amount. 1st cycle coulombic efficiency of the HC, SPC/HC90, SPC/HC70 and SPC/HC50 are 67.3%, 68.6%, 73.2% and 68.8%, respectively. The capacity retention ratios of the HC, SPC/HC90 and SPC/HC70 composites are as high as 94.9%, 94.2%, and 83.2% after 30 cycles, whereas, that of the SPC/HC50 is as low as 59.9%, respectively. The improvement of cyclability can be explained by the composite structure, in which SPC particles are embedded, so that the contact area between SPC and the electrolyte is decreased. The Si embedding is well known to enhance the cyclability, because they protect a separation of Si particles from conductive paths by increasing cycles [16].

The rate performance of the HC and SPC/HC composites is plotted as functions of current in figure 3 (b). The composition of SPC into HC on rate performance of the HC and SPC/HC composites is evaluated under charge at 30 mA g^{-1} and discharge at variable current. The discharge capacity of the HC gradually decreases with an increasing the current from 30 mA g^{-1} to $1,500 \text{ mA g}^{-1}$. The discharge capacity of the HC is not able to be measured above $3,000 \text{ mA g}^{-1}$ due to the destruction of the electrode. The SPC/HC90 and SPC/HC70 composites show much improved rate performance up to $3,000 \text{ mA g}^{-1}$, compared to the HC. It is indicated that the composition of SPC into HC successfully improved rate performance. For the SPC/HC50 composite, however, rate performance decreases drastically with an increase of the current. In a previous study, improvement electrochemical

performance of a Si/carbon nanofiber composite (SPC) was due to CNF on the surface of the silicon particles, which suppressed volume expansion by providing adequate internal space in the electrode [17]. Therefore, this internal space of SPC can be changed to internal pore in SPC/HC composites during composite processes using SPC and EO-derived pitch in Figure 1. In table 1, a large amount of the internal pore volume is developed in SPC/HC composites. This implies that the internal pore volume of HC itself is not sufficient to enhance the rate performance over $3,000 \text{ mA g}^{-1}$. However, the internal pore volumes of SPC/HC90 and SPC/HC70 are sufficient to enhance the rate performance over $3,000 \text{ mA g}^{-1}$, whereas, that of SPC/HC50 could cause a side effect on rate performance due to much quantity as 50% of SPC.

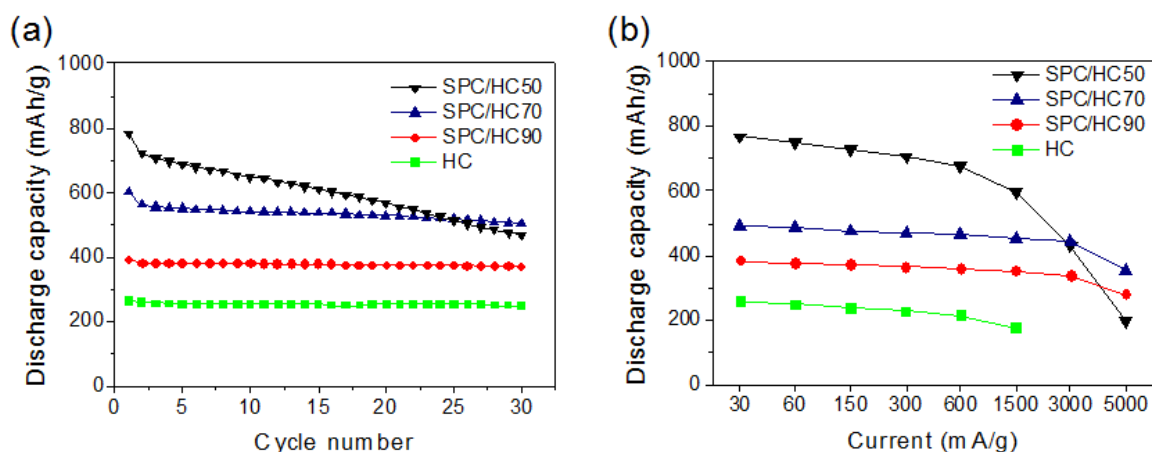


Figure 3. The cyclability and rate performance of the HC and SPC/HC composites.

3.3. Volume expansion and SEM images after rate test

The ratio of volume expansion is estimated for four different states of electrode in figure 4 (a). The first state is prepared by the impregnation of the electrode in the electrolyte solution for 2 days at room temperature after coin cell assembling. The second one is after being charged at the first cycle to 0 V. The third one is after 30 cycles test and last one was after rate test from 30 mA g^{-1} to 5000 mA g^{-1} . Regardless of active materials, the volumetric expansion ratios (changed thickness / initial thickness $\times 100$ (%)) of the impregnated electrode are almost comparable, 110–116%. After being charged at the first cycle to 0 V, the electrodes of SPC/HC70 and SPC/HC50 are shown larger volume expansion of 126% and 141%, respectively, than those of HC and SPC/HC90 of 118% and 117%, respectively. After the 30 cycles test, the electrodes of SPC/HC70 and SPC/HC50 are shown remarkably large volume expansion of 137% and 197%, whereas HC and SPC/HC90 showed relatively low volume expansion of 120% and 122%, respectively. And after the rate test, the electrodes of SPC/HC70 and SPC/HC50 are shown also obviously large volume expansion of 168% and 196%, respectively. Especially, the electrode of SPC/HC90 after rate test are shown the smallest volume expansion of 127%, even less than that of HC electrode (136%).

Figure 4 (b)–(e) shows surface SEM images of the HC and SPC/HC composites after rate test at 5,000 mA g⁻¹. Figure 4 (b) shows that the electrode of HC was destructed after rate test. However, the electrodes of SPC/HC90 and SPC/HC70 show the homogeneous surface morphology and no remarkable cracks after rate test even at 5,000 mA g⁻¹ in figure 4 (c) and (d). In figure 4 (e), the electrode of SPC/HC50 shows some cracks on the surface after rate test. These imply that the internal pores of the SPC/HC composites could suppress the crack propagation due to the volume expansion of the anodes at high C-rates and maintain the connectivity in the electrode. However, that of SPC/HC50 composite could not relax the crack propagation because of much quantity of SPC as 50%.

The good electrochemical performance of SPC/HC composites can be ascribed to the buffering effect of internal pore, which provides facile strain relaxation during electrode structure changes by the large Si volume expansion during cycles and to the electronic contact through carbon nanofiber between Si and hard carbon matrix [14]. As a result, SPC/HC composites show synergy effect from both Si/carbon nanofiber phase and hard carbon matrix.

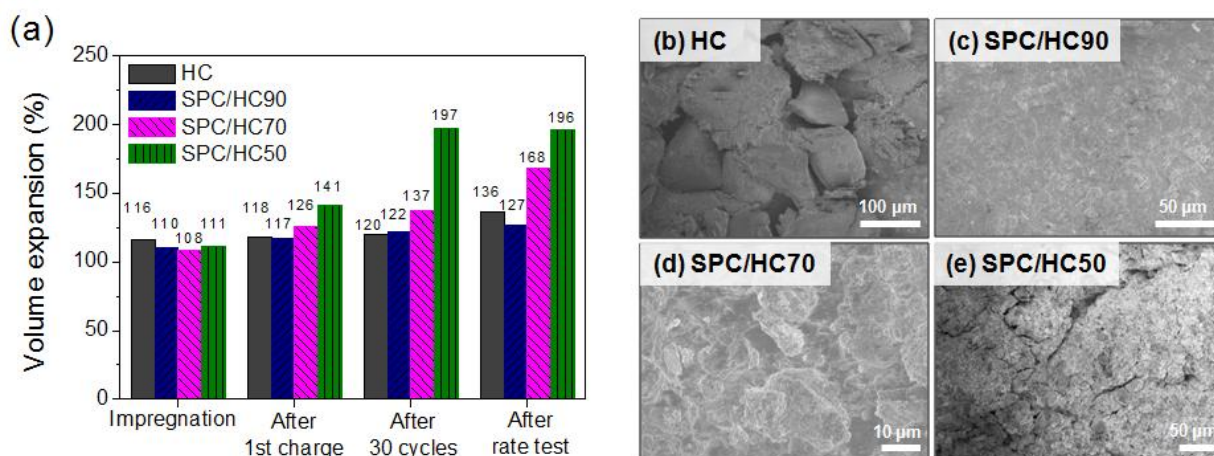


Figure 4. Volume expansion ratios after impregnation, first cycle charge, 30 cycles, rate test (a) and surface SEM images (b) - (e) of the HC and SPC/HC composites after rate test at 5,000 mA g⁻¹.

4. CONCLUSION

The composition effect of SPC into HC for the application of Li-ion battery has been evaluated in terms of discharge rate performance. The internal pore volume in the SPC/HC composites is efficiently increased via the composition of SPC into HC matrix. The introduced internal pores relieve the crack propagation of the anodes and suppress the volume expansion of the electrodes at high C-rates. Thus, the introduced internal pores of SPC/HC compositions afford to show the high discharge rate performance, better cyclability and reasonable 1st cycle coulombic efficiency, which are core requirements for high power Li-ion battery applications. It is important to control internal pore volume with appropriate composition ratio because the excessive addition of SPC into the HC matrix has adverse effects on the electrochemical properties.

ACKNOWLEDGMENTS

This research was carried out within the categories of the Global-Center of Excellence (G-COE) in Novel Carbon Resource Sciences of Kyushu University and ALCA program of JST. The present authors are sincerely appreciated to their financial supports.

References

1. R. F. Liang, Z. X. Wang, H. J. Guo, X. H. Li, W.J. Peng, Z. G. Wang, *J. Power Sources* 184 (2008) 598
2. R. Yazami, M. Deschamps, *J. Power Sources* 54 (1995) 411
3. T. Zheng, W. Xing, J. R. Dahn, *Carbon* 34 (1996) 1501
4. E. Buiel, J. R. Dahn, *Electrochim. Acta* 45 (1999) 121
5. P. R. Bueno, E. R. Leite, *J. Phys. Chem. B* 107 (2003) 8868
6. F. Cheng, Z. Tao, J. Liang, J. Chen, *Chem. Mater.* 20 (2008) 667
7. C. Li, X. Yin, L. Chen, Q. Li, T. Wang, *J. Phys. Chem. C* 113 (2009) 13438
8. F. Zhang, K. X. Wang, G. D. Li, J. S. Chen, *Electrochem. Commun.* 11 (2009) 130
9. J. Yi, X. P. Li, S. J. Hu, W. S. Li, L. Zhou, M. Q. Xu, J. F. Lei, L. S. Hao, *J. Power Sources* 196 (2011) 6670
10. J. Yang, X. Zhou, Y. Zou, J. Tang, *Electrochim. Acta* 56 (2011) 8576
11. Z. Hou, F. Zeng, B. He, W. Tao, C. Ge, Y. Kuang, J. Zeng, *Mater. Lett.* 65 (2011) 897
12. C. Kim, K.S. Yang, M. Kojima, K. Yoshida, Y.J. Kim, Y.A. Kim, M. Endo, *Adv. Funct. Mater.* 16 (2006) 2393
13. Y. S. Hu, R. Demir-Cakem, M. Titirici, J. Muller, R. Schlogl, M. Antonitti, J. Maier, *Angew. Chem. Int. Ed.* 47 (2008) 1645
14. L. Ji, X. Zhang, *Electrochem. Commun.* 11 (2009) 1146
15. M. Ruike, T. Kasu, N. Setoyama, T. Suzuki, K. Kaneko, *J. Phys. Chem.* 98 (1994) 9594
16. H. Li, L. Shi, Q. Wang, L. Chen, X. Hunag, *Solid State Ionics* 148 (2002) 247
17. S. Jang, J. Miyawaki, M. Tsuji, I. Mochida, S. Yoon, *Carbon* 47 (2009) 3383